

Research Article

Epitaxial growth of Pd clusters on N-doped Ag nanowires for oxygen reduction reaction

 Qinhe Guan^a, Shiwei Sun^a, Xiaohang Ge^a, Fan Zhang^a, Lijie Qu^a, Chao Yin^a,
 Weiyong Yuan^{b,c,*}, Lianying Zhang^{a,*}
^a Institute of Materials for Energy and Environment, College of Materials Science and Engineering, Qingdao University, Qingdao 266071, China^b Ningbo Innovation Centre, Zhejiang University, Ningbo 315100, China^c College of Chemical and Biological Engineering, Zhejiang University, Hangzhou 310027, China

ARTICLE INFO

Keywords:

 N doping
 Epitaxial growth
 PdAg heterostructure
 Ag nanowires
 Oxygen reduction

ABSTRACT

Efficient and stable Pt-free electrocatalysts for oxygen reduction reaction (ORR) are indispensable for future fuel cells. Herein, we describe a heterostructure of Pd nanocrystals (PdNCs) on N-doped Ag nanowires (NWs) synthesized using a direct epitaxial growth strategy with a Pd loading of only 9.5 wt.%. The PdAg bimetallic heterostructure showed the highest mass activity among reported PdAg-based ORR electrocatalysts and exhibited excellent stability, with only a 1.5 mV decay in the half-wave potential even after 20000 cycles of continuous testing. The remarkably enhanced activity and durability can be attributed to the distinct advantages of the ultrasmall PdNCs, cocatalysts of N-doped AgNWs, and their heterointerfaces. This work reveals that the epitaxial growth of a heterostructure on a stable support is a promising strategy for promoting catalytic performance.

1. Introduction

Fuel cells have long been developed as an ideal solution for future vehicles [1–3]; however, their practical performance is severely restricted by the sluggish reaction kinetics of the cathodic oxygen reduction reaction (ORR) [4,5]. Pt is the most studied electrocatalyst for the ORR, but it suffers from scarcity, high cost, and unsatisfactory stability, hampering its large-scale application [6,7]. In recent decades, a series of Pt-free catalysts, including non-noble metals, heteroatom-doped carbon materials, and metal nitrides, have been developed. However, their durability usually does not satisfy the requirements for future applications [8–12]. Pd is a viable substitute for Pt because it has 50 times more reserves, a similar electronic structure, and comparable ORR activities [13,14]. Although tremendous progress has been made in the development of Pd-based ORR catalysts [15–19], more effort should be devoted to reducing Pd usage while improving its catalytic properties.

The construction of Pd-based bimetallic structures is an effective solution to boost the ORR performance of Pd while increasing its utilization, owing to the synergetic effects between the two metallic components, which contribute to the optimization of the electronic state of Pd [20–23]. To date, significant advances have been made in the preparation of Pd-based bimetallic nanocrystals (NCs) with various morphologies and compositions [24–26]. In particular, PdAg bimetallic catalysts

have received extensive attention for the ORR [27–30]. Ag is more than 100 times more abundant than Pd and has distinct ORR activity in alkaline media [31,32]. Compared to non-noble transition metals, Ag has higher electrical conductivity and a much more positive equilibrium electrode potential; therefore, it could be a promising catalyst support with better structural stability [33]. Nevertheless, considering the harsh operating conditions of fuel cells, the structural stability of the catalysts needs to be further improved [34,35]. Recent reports have revealed that the electrochemical stability of transition metals can be enhanced by N-doping, which can fine-tune the electronic state of the metallic component, contributing to the transfer of charges from the N atom to the coordinated metal atom [36,37]. Support corrosion is a problem for systems that disperse NC catalysts directly on carbon-based supports, including activated carbon, carbon nanotubes, and graphitized carbons [1,38,39]. In addition, the limited anchoring points between the NC catalysts and the carbon support, along with their weak interactions, make the catalysts relatively mobile and thus prone to aggregation, resulting in a deterioration in activity and stability [40].

In this work, we report an advanced Pt-free electrocatalyst prepared via the direct epitaxial growth of PdNCs on N-doped Ag nanowires (PdNCs/N-AgNWs). The PdNCs were uniformly dispersed on the N-doped AgNWs, with a size in the range of 3–5 nm and a Pd loading of only 9.5 wt.%. In the ORR, the PdNCs/N-AgNWs heterostructure

* Corresponding authors.

E-mail addresses: wuyuan@zju.edu.cn (W. Yuan), lyzhang@swu.edu.cn (L. Zhang).<https://doi.org/10.1016/j.chphma.2024.06.004>

Received 6 February 2024; Received in revised form 26 May 2024; Accepted 14 June 2024

Available online 24 June 2024

2772-5715/© 2024 The Authors. Publishing Services by Elsevier B.V. on behalf of KeAi Communications Co. Ltd. This is an open access article under the CC BY-NC-ND license (<http://creativecommons.org/licenses/by-nc-nd/4.0/>)

shows remarkably higher activity and durability compared to PdNCs on AgNWs without N doping (PdNCs/AgNWs) and commercial Pd/C (Com Pd-C) catalysts. Structural characterization and electrochemical measurements indicate that the synergetic effect between the N-AgNWs and PdNCs, along with the epitaxial heterointerfaces, play major roles in the catalysis enhancement.

2. Experimental

2.1. Preparation of AgNWs and N-doped AgNWs

AgNWs were obtained using a modified polyol approach. First, 750.0 mg of polyvinyl pyrrolidone (PVP, MW = 40000) was added to 25.0 mL of glycerol and continuously stirred at 85 °C for 12 h. Next, 200.0 mg of silver nitrate was dissolved in 1.5 mL of ethylene glycol and then transferred into the above solution. After stirring for 15 min, 75 μ L of NaCl solution, with a concentration of 100 mg mL⁻¹, was slowly added to the mixture. The resulting viscous solution was heated to 180 °C for 4 h under stirring. After cooling to room temperature (25 \pm 5 °C), the product was transferred to excess ammonium hydroxide and stirred for 30 min, followed by washing several times with deionized water and ethanol. Finally, 20.0 mg of collected AgNWs and 400.0 mg of urea were added to 30.0 mL of ethanol and stirred for 30 min. Then, the mixture was transferred into a high-pressure reactor and heated at 180 °C for 2 h. After cooling to room temperature, the product was washed twice with deionized water and twice with ethanol in sequence. The collected gray precipitate was denoted as N-AgNWs.

2.2. Preparation of PdNCs/AgNWs and PdNCs/N-AgNWs

10.0 mg of N-AgNWs (or AgNWs) was dispersed into 15.0 mL of deionized water and stirred for 10 min while being heated at 50 °C. Next, 2.0 mg of ammonium tetrachloride palladium was dissolved into 1.0 mL of deionized water, and this solution was injected into the mixture. After stirring for 15 min, the precipitate was collected and washed thrice with deionized water. The resulting product was named PdNCs/N-AgNWs (or PdNCs/AgNWs).

2.3. Electrochemical measurements

5.0 mg of the prepared PdNCs/N-AgNWs and 20.0 mg of Vulcan XC-72 carbon were dispersed in a mixture of ethanol (18.3 mL), deionized water (6.0 mL), and Nafion solution (0.7 mL, 0.5 wt.%) under ultrasonication for 40 min. Then, 10.0 μ L of the catalyst ink was dropped onto a rotating disk electrode (diameter: 5.0 mm), which served as the working electrode. A graphite rod and a Hg/HgO electrode (containing 1.0 M NaOH solution) were used as the counter and reference electrodes, respectively. The Pd loading on the working electrode was 0.97 μ g cm⁻²_{Pd}. All electrochemical experiments were performed on an electrochemical workstation (CHI760E) using a typical three-electrode testing system. Cyclic voltammetry (CV) profiles were measured in a nitrogen-saturated 0.1 M KOH solution at a scan rate of 50 mV s⁻¹. Polarization profiles were measured in an oxygen-saturated 0.1 M KOH solution at a rotation rate of 1600 rpm and a scan rate of 5 mV s⁻¹. All electrochemical tests were performed at room temperature.

3. Results and discussion

3.1. Morphology and nanostructure of PdNCs/N-AgNWs

Figs. 1(a)–(c) show representative scanning electron microscopy (SEM) images of the AgNWs, N-AgNWs, and PdNCs/N-AgNWs, respectively. The AgNWs have a length exceeding 500 nm and a diameter of 50 \pm 2 nm. The lengths and diameters of the N-AgNWs were similar to those of the AgNWs (Fig. 1(b)), suggesting that the N-doping treatment was mild. Both the AgNWs and N-AgNWs exhibited smooth surfaces.

After the direct epitaxial growth of PdNCs on N-AgNWs, the diameter of product increased to 53 \pm 2 nm (Fig. 1(c)). Figs. 1(d)–(g) show transmission electron microscopy (TEM) images of the PdNCs/N-AgNWs at different magnifications. The PdNCs were uniformly distributed on the N-AgNWs (or AgNWs), and the crystal sizes were approximately in the range of 3–5 nm (Figs. 1(d)(e) and S1). This finding demonstrates the negligible effect of the N dopant in the AgNWs on the crystal size and dispersity of the PdNCs. The distinct lattice fringes in Fig. 1(f) demonstrate the high crystallinity of the obtained N-AgNWs, with an adjacent lattice spacing of 0.233 nm corresponding to the Ag(111) facets [41]. The continuous lattice fringes from the N-AgNWs to the PdNCs suggest that the PdNCs grew epitaxially on the N-AgNWs (Fig. 1(g)). For the Pd NC in Fig. 1(g), the adjacent lattice spacing of 0.225 nm can be assigned to the Pd(111) facets [42], which is close to the value of the Ag(111) facets, with only a 3.4% difference in lattice mismatch. The direct epitaxial growth of PdNCs on N-AgNWs likely arises from the more positive redox potential of PdCl₄²⁻/Pd⁰ (0.591 V vs. RHE) relative to Ag⁺/Ag⁰ (0.490 V vs. RHE), leading to the galvanic displacement reaction between Ag and PdCl₄²⁻ [43]. A small lattice mismatch between Pd and Ag is believed to be indispensable for direct epitaxial growth [44–46]. The two clear and symmetrical diffraction spots in the inset of Fig. 1(g) demonstrate the high crystallinity of the PdNC, which is consistent with the TEM analysis in Fig. 1(f). The heterointerface in the PdNCs/N-AgNWs helps limit mobility, aggregation, and Ostwald ripening through the confinement effect, thus ensuring high structural stability [47,48].

The X-ray diffraction (XRD) pattern of the PdNCs/N-AgNWs was recorded to obtain additional structural information (Fig. 2(a)). For comparison, XRD patterns of the AgNWs, N-AgNWs, and PdNCs/AgNWs were also recorded. The strong diffraction peaks at 37.85°, 44.14°, 64.25°, 77.22°, and 81.40° correspond to the Ag (111), Ag (200), Ag (220), Ag (311), and Ag (222) planes, respectively [49]. The Ag (200) planes of the N-AgNWs shifted by 0.3° to more positive positions compared to those of the AgNWs, indicating a lattice contraction upon N-doping [50]. This result suggests the successful doping of N into Ag crystals [51]. The diffraction peaks of PdNCs/AgNWs and PdNCs/N-AgNWs were located between those of AgNWs (or N-AgNWs) and Pd crystals (JCPDS: 46–1043), demonstrating the formation of a PdAg bimetallic structure. In comparison with AgNWs, the X-ray photoelectron spectroscopy (XPS) spectrum of the Ag 3d peaks of N-AgNWs shows an obvious positive shift (Fig. 2(b)), confirming the doping of N into the Ag crystal. This shift occurs because of electrons transfer from Ag to N, driven by the high electronegativity of N [36,52]. This result indicates the significant role of N dopant modifying the electronic state of Ag. Fig. 2(c) shows the XPS spectrum of N 1s for PdNCs/N-AgNWs, revealing the presence of two types of N-based species on their surfaces. The prominent N 1s peak at 398.6 eV corresponds to N-Ag bonding, suggesting a strong interaction between Ag and the dopant N. The peaks at 400.5 and 404.0 eV are related to amino N and oxynitride, respectively [53]. For PdNCs/AgNWs and PdNCs/N-AgNWs, the Ag 3d peaks were negatively shifted compared to the Ag 3d peaks of AgNWs (or N-AgNWs). Specifically, the Ag 3d peaks of PdNCs/N-AgNWs exhibit a 0.3 eV shift to more negative positions compared to those of PdNCs/AgNWs (Fig. 2(d)). In contrast, the Pd 3d peaks of both heterostructures were positively shifted compared to the Pd 3d peaks of Com Pd-C. Importantly, the Pd 3d peaks of PdNCs/N-AgNWs show 0.2 eV positive shift compared to those of PdNC/AgNWs (Fig. 2(e)). These results revealed that the epitaxial growth of PdNCs on AgNWs (or N-AgNWs) significantly alters the electronic states of Pd and Ag, with electrons transferred from Pd to Ag through the heterointerfaces. The electronic state of Pd in PdNC/N-AgNWs was optimized by N doping. The atomic ratio of Pd/Ag, determined by inductively coupled plasma-optical emission spectrometry, is 9.6/90.4, indicating a Pd loading of only 9.5 wt.% in PdNCs/N-AgNWs. The direct epitaxial growth of PdNCs on N-AgNWs via a galvanic displacement reaction is schematically shown in Fig. 2(f).

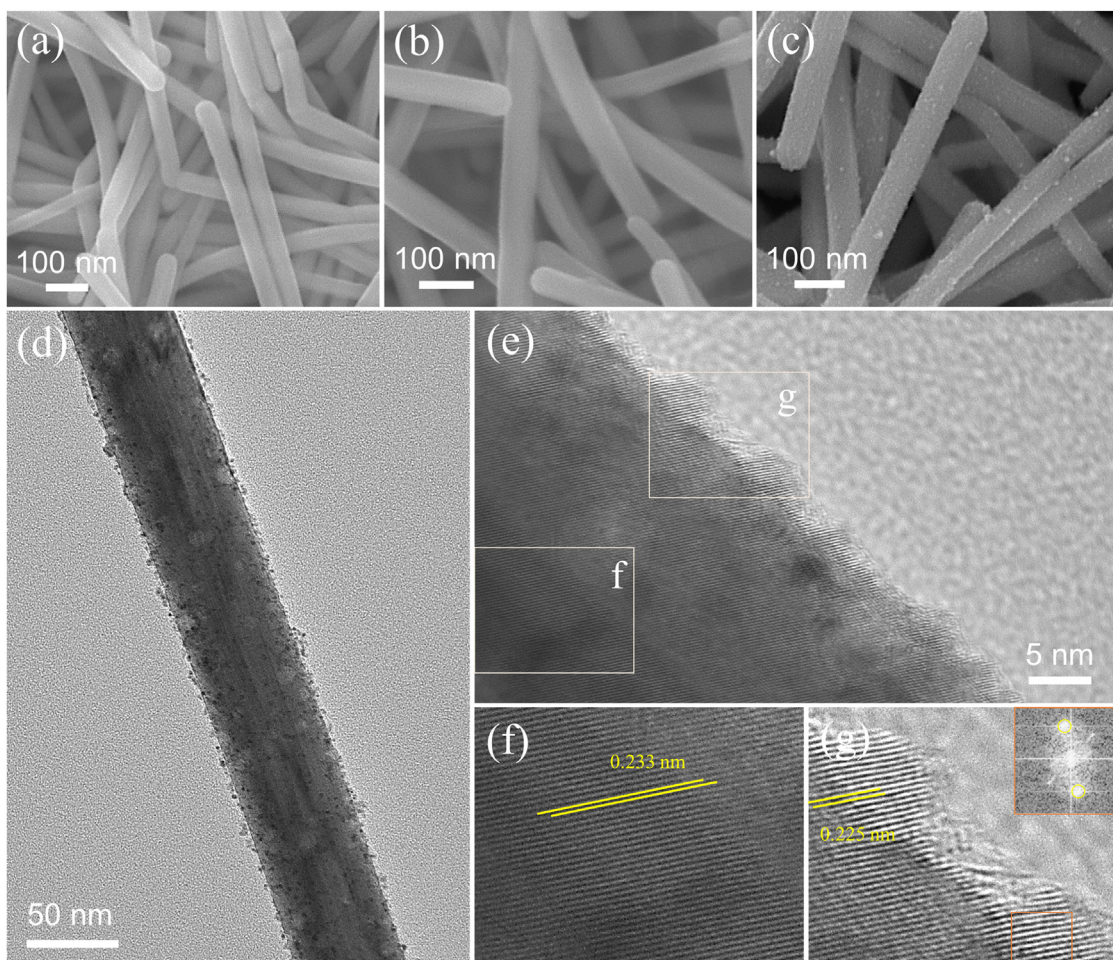


Fig. 1. SEM images of (a) AgNWs, (b) N-AgNWs, and (c) PdNCs/N-AgNWs. (d)–(g) TEM images of PdNCs/N-AgNWs. The inset in (g) is the fast Fourier transform pattern from the region marked with a brown border, confirming the crystalline structure.

3.2. Electrochemical studies of PdNCs/N-AgNWs in the ORR

To understand the electrochemical behavior of PdNCs/N-AgNWs/C towards the ORR, a polarization curve was recorded (Fig. 3(a)). The polarization curves of PdNCs/AgNWs/C and Com Pd-C were measured for comparison. For the ORR, the half-wave potential serves as an indicator to assess the catalytic activity of an electrode, and can be determined by the potential at half of the diffusion-limited current density [54,55]. In general, a positive half-wave potential indicates a high activity in the ORR. PdNCs/AgNWs/C exhibited a half-wave potential of 0.842 V, which was 14 mV more positive than that of Com Pd-C (0.828 V). For PdNCs/N-AgNWs/C, the half-wave potential was as high as 0.854 V, which is 13 mV higher than that of PdNC/AgNWs/C. These results demonstrate the significant catalytic activity of PdNCs/N-AgNWs/C in the ORR. Both the N dopant and the heterointerface between PdNCs on the N-AgNWs contribute to enhancing ORR activity. To gain further insights into the effects of the N dopant and AgNWs on PdNCs/N-AgNWs/C, the polarization curves of AgNWs/C and N-AgNWs/C were also recorded. The half-wave potential of AgNW/C was 0.700 V, and the half-wave potential of N-AgNW/C shifted to 0.718 V (Fig. S2). This result demonstrates that N-AgNWs can serve not only as a support for PdNCs but also as a cocatalyst for the ORR. The Tafel slopes of PdNCs/N-AgNWs/C, PdNCs/AgNWs/C, and Com Pd-C are 76.7, 78.3, and 81.1 mV dec^{-1} , respectively. The small Tafel slope of PdNCs/N-AgNWs/C implies fast reaction kinetics (Fig. 3(b)) [56]. Interestingly, PdNCs/N-AgNWs/C exhibits a mass activity of $1.68 \text{ A mg}^{-1}_{\text{Pd}}$, which is 12.0- and 1.7-fold higher than those of Com Pd-C ($0.14 \text{ A mg}^{-1}_{\text{Pd}}$) and PdNCs/AgNWs/C ($0.98 \text{ A mg}^{-1}_{\text{Pd}}$) (Fig. 3(c)). Moreover, PdNCs/N-AgNWs/C shows a spe-

cific activity of $1.62 \text{ mA cm}^{-2}_{\text{Pd}}$, significantly higher than the values for Com Pd-C ($0.26 \text{ mA cm}^{-2}_{\text{Pd}}$) and PdNCs/AgNWs/C ($0.96 \text{ mA cm}^{-2}_{\text{Pd}}$). To the best of our knowledge, PdNCs/N-AgNWs/C shows the most positive half-wave potential and the highest mass activity in the ORR among reported PdAg bimetallic catalysts. A comparison of half-wave potential and mass activity between PdNCs/N-AgNWs/C and representative PdAg bimetallic catalysts is summarized in Table S1. For PdNCs/N-AgNWs/C, the current density increased with increasing rotation rate due to the shortened diffusion layer length and accelerated transport of dissolved oxygen [57]. Fundamentally, the electron transfer number (n) per oxygen molecule can be calculated from the slopes of Koutecky–Levich plots. The fitting lines with high linearity and approximate parallelism suggest a similar value of n for PdNCs/N-AgNWs/C in the ORR (Fig. 3(d)). The calculated n value is 3.85, demonstrating the predominant four-electron transfer pathway in the ORR. Furthermore, the rotating ring-disk electrode test in Fig. S3 revealed that the ORR process on PdNCs/N-AgNWs/C primarily proceeds through the four-electron pathway, with a low yield of HO_2^- .

In addition to catalytic activity, stability is another key factor determining the potential of a catalyst for practical applications. An accelerated stability test using continuous CV was conducted to verify the durability of PdNCs/N-AgNWs/C in the ORR, with PdNCs/AgNWs/C and Com Pd-C as control samples. For PdNCs/N-AgNWs/C, only a slight 1.5 mV drop in the half-wave potential was observed after 20000 cycles of testing (Fig. 4(a)). In contrast, the drop for PdNCs/AgNWs/C increased to 8 mV (Fig. 4(b)), indicating a higher degree of degradation compared to PdNCs/N-AgNWs/C. Moreover, Com Pd-C exhibited a substantial half-wave potential decay of 15 mV (Fig. S4). The minimal

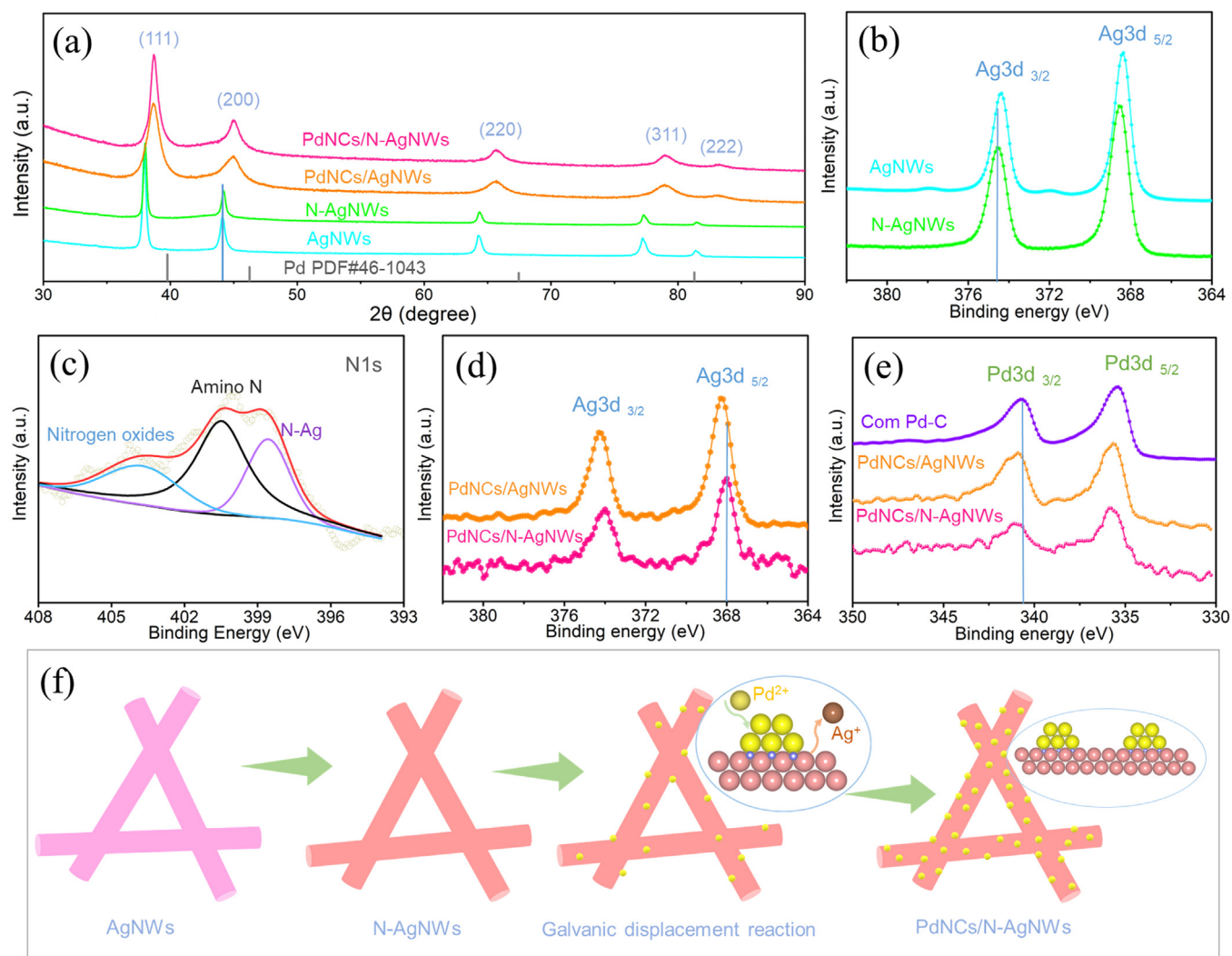


Fig. 2. (a) XRD pattern showing diffraction peaks of AgNWs, N-AgNWs, PdNCs/AgNWs, and PdNCs/N-AgNWs. (b) XPS spectra of Ag 3d for AgNWs and N-AgNWs. (c) XPS spectrum of N 1s for PdNCs/N-AgNWs. XPS spectra of (d) Ag 3d and (e) Pd 3d for PdNCs/AgNWs and PdNCs/N-AgNWs. (f) Schematic representation of the epitaxial growth process of PdNCs on N-AgNWs.

degradation observed in PdNCs/N-AgNWs/C demonstrates its excellent stability in the ORR. The excellent stability of PdNCs/N-AgNWs/C was confirmed by examining the normalized mass activity evolution of the three Pd-based catalysts (Fig. 4(c)). After 20000 cycles, Com Pd-C retained only 82.1% of its initial mass activity, while PdNCs/AgNWs/C increased slightly to 86.2%. Remarkably, PdNCs/N-AgNWs/C retained 96.5% of its initial mass activity, indicating superior stability compared to the other catalysts. To further understand the excellent stability of PdNCs/N-AgNWs, continuous CV tests were conducted on AgNWs/C and N-AgNWs (Figs. 4(d)(e)). For N-AgNWs, the negligible decay in the reduction peak of surface oxides demonstrated that the N dopant in the Ag crystal significantly suppresses the oxidative dissolution of Ag [58]. The uniform distribution of PdNCs on the AgNWs (Fig. 4(f)) demonstrates their remarkable structural stability. These observations reveal that both the Ag-N bonding and epitaxial heterointerfaces between PdNCs and N-AgNWs significantly contribute to enhancing the durability of PdNCs/N-AgNWs/C.

3.3. Catalysis enhancement mechanism discussion

Considering the unique structure of PdNCs/N-AgNWs and their outstanding electrochemical performance in the ORR, we argue that the substantially enhanced activity and durability can be ascribed to syner-

getic effects among the N-AgNWs, PdNCs, and epitaxial heterointerfaces (Fig. 5). The N dopant plays a critical role in activating and improving the ORR activity of AgNWs. Additionally, due to the high electrical conductivity of Ag crystals, N-AgNWs serve as favorable cocatalysts for PdNCs. In addition, the heterointerfaces between the PdNCs and N-AgNWs greatly optimized the electronic state of Pd, contributing to a significant positive shift in the binding energies of the Pd 3d peaks observed in PdNCs/N-AgNWs. Previous studies have revealed that such a positive shift in Pd binding energies results in a downshift of the d-band center, which in turn weakens the interaction of adsorbates [2,59]. Typically, the Pd surface exhibits strong adsorption energies for oxygen species (O^*), which can hinder the oxidative adsorption of hydroxides and limit the ORR kinetics [2]. Ag exhibited significantly weak binding to O^* [60]. According to the classical d-band model, which describes the interaction between the catalyst surface and intermediate adsorption, moderate adsorption of intermediates is critical for favorable ORR activity [61,62]. Therefore, the greatly enhanced ORR activity of PdNCs/N-AgNWs can be attributed to the synergistic co-catalytic effect of N-AgNWs and the heterointerfaces between PdNCs and N-AgNWs. These factors collectively regulate the electronic state of Pd, leading to a weakening of the O^* adsorption strength. Regarding the stability of PdNCs/N-AgNWs, the strong N-Ag bonding significantly regulates the electronic state of Ag [53], thereby suppressing the oxidative dissolution of Ag and enhancing

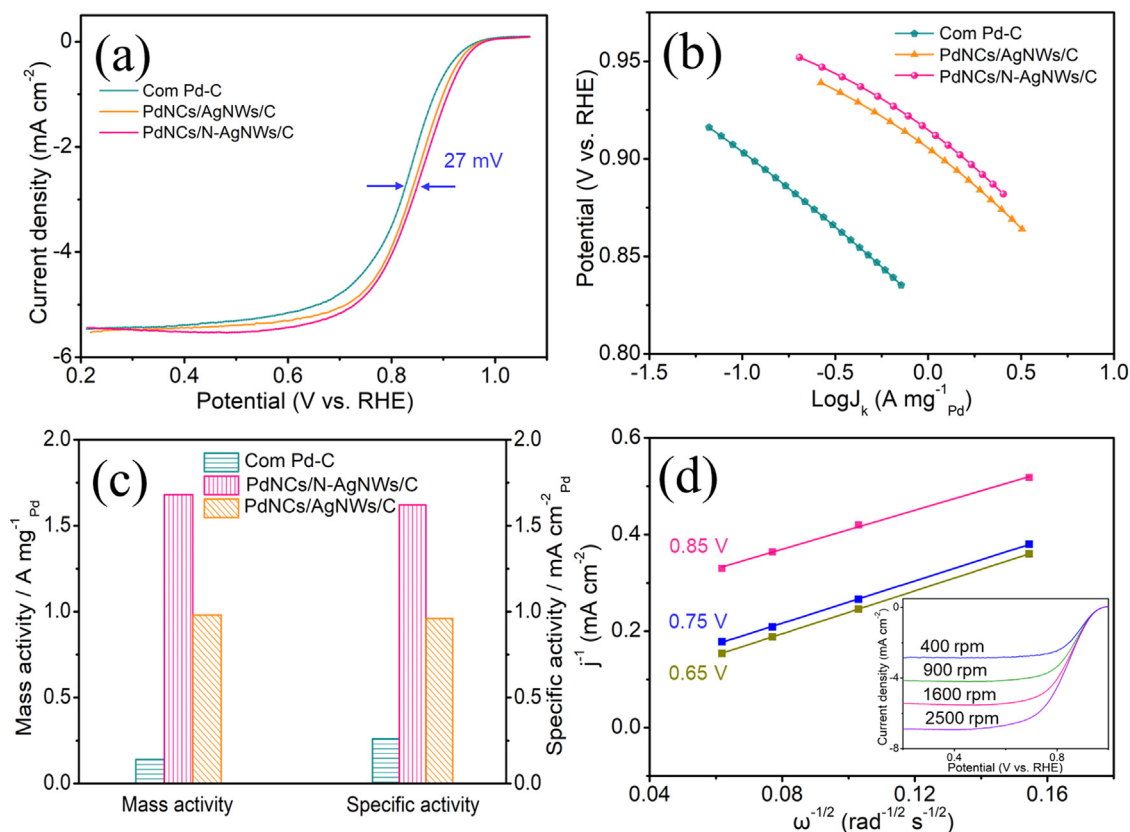


Fig. 3. (a) Polarization profiles of electrocatalysts. (b) Tafel plots and (c) activity (at 0.9 V) of PdNCs/N-AgNWs/C and control samples. (d) Linear sweep voltammetry profiles of PdNCs/N-AgNWs/C at different rotation speeds and corresponding Koutecky-Levich plots at 0.65, 0.75, and 0.85 V (vs. RHE).

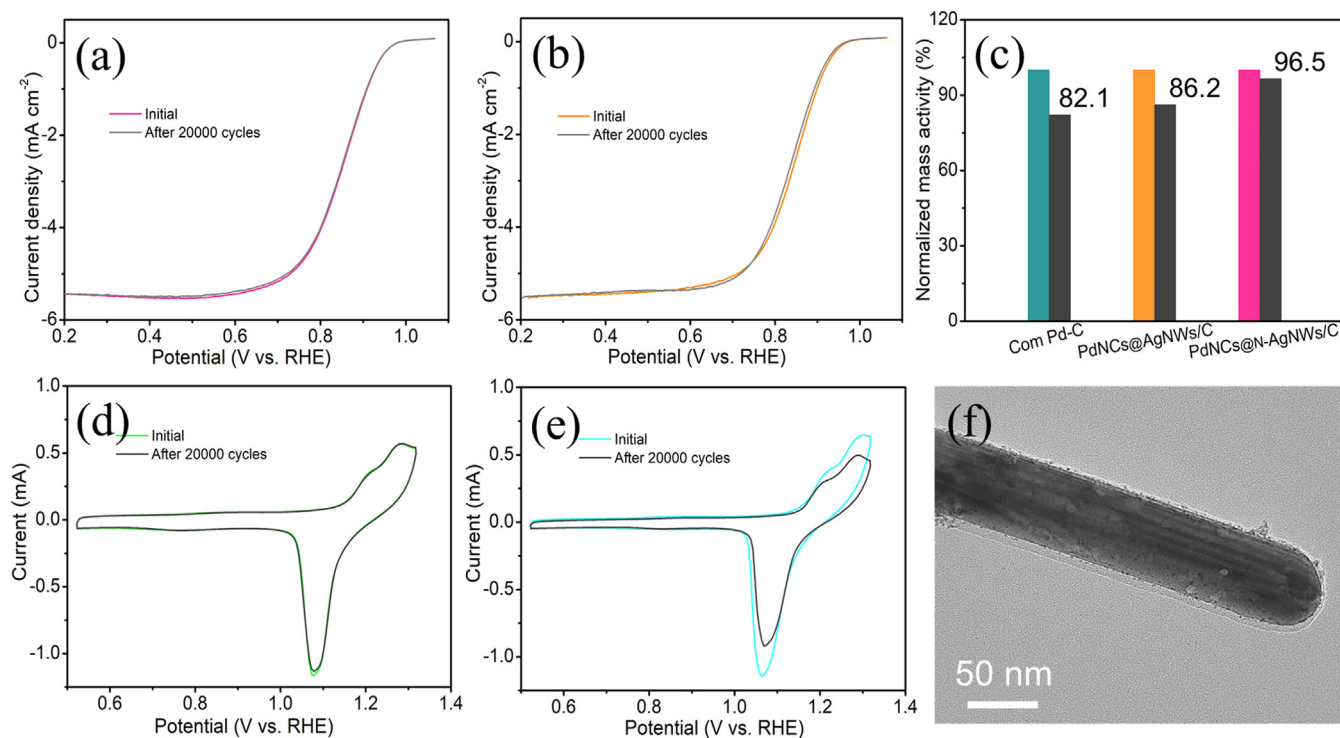


Fig. 4. Polarization profiles of (a) PdNCs/N-AgNWs/C and (b) PdNCs/AgNWs/C before and after durability tests. (c) Mass activity evolution for various Pd-based catalysts at 0.9 V (vs. RHE). CV curves of (d) N-AgNWs/C and (e) AgNWs/C before and after durability tests. (f) TEM image of PdNCs/N-AgNWs/C after durability testing.

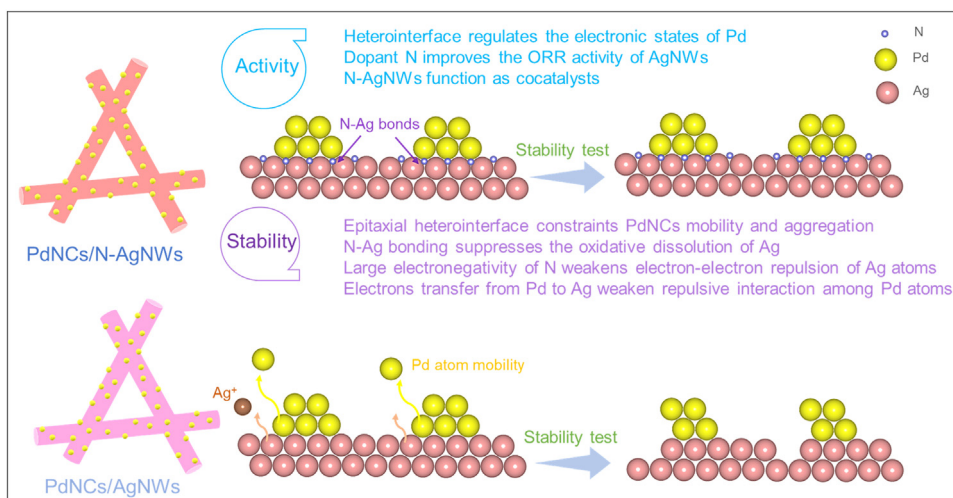


Fig. 5. Schematic illustration of the catalytic enhancement mechanism of PdNCs/N-AgNWs toward the ORR.

the stability of N-AgNWs as a support material. Compared to pure Ag, N possesses a higher electronegativity, which promotes electron transfer from Ag to N. It is believed that this electron transfer reduces electron-electron repulsion among Ag atoms, contributes to the structural stability of N-AgNWs. In the case of PdNCs/N-AgNWs, electrons transferred from Pd to Ag at the epitaxial heterointerfaces between N-AgNWs and PdNCs further weaken electron repulsive interactions among Pd atoms. Moreover, these heterointerfaces effectively limit the mobility of small-sized PdNCs, preventing their aggregation and maintaining high structural stability through crystal confinement [48]. Both factors contribute significantly to enhanced stability. The uniform dispersion of PdNCs helps suppress Ostwald ripening [63]. Additionally, PdNCs/N-AgNWs with Pd loadings as low as 9.5 wt.% can be readily prepared through epitaxial growth, making them well-suited for mass production. Therefore, PdNCs/N-AgNWs hold great potential as ORR catalysts in fuel cells.

4. Conclusions

We report a Pt-free ORR catalyst consisting of PdNCs epitaxially grown on N-doped AgNWs. The PdNCs were uniformly dispersed on the N-doped AgNWs, featuring sizes in the range of 3–5 nm and a Pd loading of only 9.5 wt.%. In ORR applications, the PdNCs/N-AgNWs heterostructure exhibits the highest mass activity of $1.68 \text{ A mg}^{-1} \text{ Pd}$ among reported PdAg bimetallic catalysts. This performance is notably superior, exhibiting 12.0- and 1.7-times higher mass activities compared to Com Pd-C and PdNCs/AgNWs, respectively. The PdNCs/N-AgNWs heterostructure also shows a 27 mV more positive potential in half-wave potential compared to Com Pd-C catalyst. In addition, it exhibits exceptional stability, with only a 1.5 mV drop in half-wave potential after 20000 cycles of testing. The increased ORR activity is primarily attributed to the N-AgNW cocatalyst and the heterointerface, which effectively regulates the electronic state of Pd. The uniform distribution of ultrasmall Pd NCs is believed to provide abundant catalytic active sites, further enhancing ORR activity. The excellent stability of the PdNCs/N-AgNWs catalyst can be attributed to several factors. First, strong N–Ag bonding effectively suppresses the oxidative dissolution of surface Ag on PdNCs/N-AgNWs. Second, the epitaxial heterointerfaces between PdNCs and N-AgNWs play a crucial role in restricting the mobility and aggregation of PdNCs through crystal confinement. In addition, the N dopant in Ag contributes to the high structural stability by mitigating the electron-electron repulsion among Ag atoms. This work offers an active and stable Pt-free electrocatalyst for the ORR, leveraging the synergistic effects of epitaxial growth of heterostructures and a durable catalyst support. By integrating these

strategies, both the activity and stability of the catalyst are enhanced, offering promising implications for catalytic applications.

Declaration of Competing Interest

The authors declare that they have no known competing financial interests or personal relationships that could have appeared to influence the work reported in this paper.

CRedit authorship contribution statement

Qinhe Guan: Writing – original draft, Investigation. **Shiwei Sun:** Software, Investigation. **Xiaohang Ge:** Investigation. **Fan Zhang:** Investigation. **Lijie Qu:** Investigation. **Chao Yin:** Investigation. **Weiyong Yuan:** Writing – review & editing, Visualization, Supervision. **Lianying Zhang:** Writing – review & editing, Supervision, Conceptualization.

Acknowledgements

We gratefully acknowledge financial support from the National Natural Science Foundation of China (22379078).

Supplementary materials

Supplementary material associated with this article can be found, in the online version, at doi:10.1016/j.cphma.2024.06.004.

References

- [1] M.K. Debe, Electrocatalyst approaches and challenges for automotive fuel cells, *Nature* 486 (2012) 43–51.
- [2] L. Wang, Z. Zeng, W. Gao, T. Maxson, D. Raciti, M. Giroux, X. Pan, C. Wang, J. Greeley, Tunable intrinsic strain in two-dimensional transition metal electrocatalysts, *Science* 363 (2019) 870–874.
- [3] F. Lin, F. Lv, Q. Zhang, H. Luo, K. Wang, J. Zhou, W. Zhang, W. Zhang, D. Wang, L. Gu, Local coordination regulation through tuning atomic-scale cavities of Pd metallene toward efficient oxygen reduction electrocatalysis, *Adv. Mater.* 34 (2022) 2202084.
- [4] S. Chen, J. Zhao, H. Su, H. Li, J. Zeng, Pd-Pt tesseracts for the oxygen reduction reaction, *J. Am. Chem. Soc.* 143 (2021) 496–503.
- [5] V. Glibin, J. Dodelet, G. Zhang, Energetics and thermodynamic stability of potential Fe(II)-hexa-aza-active sites for O_2 reduction in PEM fuel cells, *SusMat* 2 (2022) 731–748.
- [6] Q.Y. Chen, Z.Y. Chen, A. Ali, Y.Q. Luo, H.Y. Feng, Y.Y. Luo, P. Tsiakaras, P.K. Shen, Shell-thickness-dependent core-shell nanosheets for efficient oxygen reduction reaction, *Chem. Eng. J.* 427 (2021) 131565.
- [7] H. Xie, S. Chen, J. Liang, T. Wang, Z. Hou, H.L. Wang, G. Chai, Q. Li, Weakening intermediate bindings on CuPd/Pd core/shell nanoparticles to achieve Pt-like bifunctional activity for hydrogen evolution and oxygen reduction reactions, *Adv. Funct. Mater.* 31 (2021) 2100883.

- [8] X. Ge, Q. Guan, F. Zhang, S. Sun, Y. Xu, K. Zhang, W. Yuan, L.Y. Zhang, Direct epitaxial growth of Au nanoparticles on Pd metallene enables robust oxygen reduction electrocatalysis, *Mater. Today Eng.* 39 (2024) 10147.
- [9] F. Zhang, S. Sun, X. Ge, Q. Guan, M. Ling, W. Yuan, L.Y. Zhang, Synthesizing Pd-based high entropy alloy nanoclusters for enhanced oxygen reduction, *Chem. Commun.* 60 (2024) 3591–3594.
- [10] T. Zeng, X. Meng, H. Huang, L. Zheng, H. Chen, Y. Zhang, W. Yuan, L.Y. Zhang, Controllable synthesis of web footed PdCu nanosheets and their electrocatalytic applications, *Small* 7 (2022) 2107623.
- [11] Y. Nie, L. Li, Z.D. Wei, Recent advancements in Pt and Pt-free catalysts for oxygen reduction reaction, *Chem. Soc. Rev.* 44 (2015) 2168–2201.
- [12] L.Y. Zhang, C.X. Guo, H. Cao, S. Wang, Y. Ouyang, B. Xu, P. Guo, C.M. Li, Highly wrinkled palladium nanosheets as advanced electrocatalysts for the oxygen reduction reaction in acidic medium, *Chem. Eng. J.* 431 (2022) 133237.
- [13] D. Yan, L. Zhang, L. Shen, R. Hu, W. Xiao, X. Yang, Pd nanoparticles embedded in N-enriched MOF-derived architectures for efficient oxygen reduction reaction in alkaline media, *Green Energy. Environ.* 8 (2022) 1205–1215.
- [14] J. Liang, Y. Xia, X. Liu, F. Huang, J. Liu, S. Li, T. Wang, S. Jiao, R. Cao, J. Han, H. Wang, Q. Li, Molybdenum doped ordered $\text{Li}_1\text{-PdZn}$ nanosheets for enhanced oxygen reduction electrocatalysis, *SusMat* 2 (2022) 347–356.
- [15] M. Zhou, J. Guo, J. Fang, Nanoscale design of Pd-based electrocatalysts for oxygen reduction reaction enhancement in alkaline media, *Small Struct.* 3 (2022) 2100188.
- [16] G. Jiang, X. Li, X. Lv, L. Chen, Core/shell FePd/Pd catalyst with a superior activity to Pt in oxygen reduction reaction, *Sci. Bull.* 61 (2016) 1248.
- [17] H. Wang, W. Wang, H. Yu, Q. Mao, Y. Xu, X. Li, Z. Wang, L. Wang, Interface engineering of polyaniline-functionalized porous Pd metallene for alkaline oxygen reduction reaction, *Appl. Catal. B-Environ.* 307 (2022) 121172.
- [18] X. Lu, M. DiSalvo, F.J. Abruna, H.D. Abruña, Enhancing the electrocatalytic activity of Pd/M (M = Ni, Mn) nanoparticles for the oxygen reduction reaction in alkaline media through electrochemical dealloying, *ACS Catal.* 10 (2020) 5891–5898.
- [19] X. Wu, C. Ni, J. Man, X. Shen, S. Cui, X. Chen, A strategy to promote the ORR electrocatalytic activity by the novel engineering bunched three-dimensional Pd-Cu alloy aerogel, *Chem. Eng. J.* 454 (2023) 140293.
- [20] C. Tan, J. Chen, X.J. Wu, H. Zhang, Epitaxial growth of hybrid nanostructures, *Nat. Rev. Mater.* 3 (2018) 17089.
- [21] T. Wang, A. Chutia, D.J.L. Brett, P.R. Shearing, G. He, G. Chai, I.P. Parkin, Palladium alloys used as electrocatalysts for the oxygen reduction reaction, *Energy Environ. Sci.* 14 (2021) 2639–2669.
- [22] Y. Zuo, D. Rao, S. Li, T. Li, G. Zhu, S. Chen, L. Song, Y. Chai, H. Han, Atomic vacancies control of Pd-based catalysts for enhanced electrochemical performance, *Adv. Mater.* 30 (2018) 1704171.
- [23] Y. Ge, X. Wang, B. Huang, Z. Huang, B. Chen, C. Ling, J. Liu, G. Liu, J. Zhang, G. Wang, Seeded synthesis of unconventional 2H-phase Pd alloy nanomaterials for highly efficient oxygen reduction, *J. Am. Chem. Soc.* 143 (2021) 17292–17299.
- [24] S. Huang, S. Lu, S. Gong, Q. Zhang, F. Duan, H. Zhu, H. Gu, W. Dong, M. Du, Sublayer stable Fe dopant in porous Pd metallene boosts oxygen reduction reaction, *ACS Nano* 16 (2022) 522–532.
- [25] H. Fu, J. Wang, Y. Chen, H. Huang, Y. Wang, H. Li, F. Lai, L. Zhang, N. Zhang, J. Chen, T. Liu, Pd_3Pb bimetallic aerogels for anti-poisoned oxygen reduction reaction, *Chem. Eng. J.* 470 (2023) 144255.
- [26] Y. Lu, J. Wang, Y. Peng, A. Fisher, X. Wang, Highly efficient and durable Pd hydride nanocubes embedded in 2D amorphous NiB nanosheets for oxygen reduction reaction, *Adv. Energy. Mater.* 7 (2017) 1700919.
- [27] D.A. Slanac, W.G. Hardin, K.P. Johnston, K.J. Stevenson, Atomic ensemble and electronic effects in Ag-rich AgPd nanoalloy catalysts for oxygen reduction in alkaline media, *J. Am. Chem. Soc.* 134 (2012) 9812–9819.
- [28] K. Park, H. Matsune, M. Kishida, S. Takenaka, Carbon-supported Pd-Ag catalysts with silica-coating layers as active and durable cathode catalysts for polymer electrolyte fuel cells, *Int. J. Hydrog. Energy* 42 (2017) 18951–18958.
- [29] L.E. Betancourt, A.R. Pérez, I. Orozco, A.I. Frenkel, Y. Li, K. Sasaki, S.D. Senanayake, C.R. Cabrera, Enhancing ORR performance of bimetallic PdAg electrocatalysts by designing interactions between Pd and Ag, *ACS Appl. Energy Mater.* 3 (2020) 2342–2349.
- [30] M.V. Cartagena, E.M. Vélez, G.S. Quintana, D.A. Pérez, M.A. Jesús, C.R. Cabrera, Silver–palladium electrodeposition on unsupported vulcan XC-72R for oxygen reduction reaction in alkaline media, *ACS Appl. Energy Mater.* 2 (2019) 4664–4673.
- [31] H. Erikson, A. Sarapu, K. Tammeveski, Oxygen reduction reaction on silver catalysts in alkaline media: A minireview, *ChemElectroChem* 6 (2019) 73–86.
- [32] Z.Z. Shi, W.P. Li, W.J. Kang, Y. Feng, Z. Li, X.Y. Zhong, J. Yang, H. Liu, C.K. Dong, P.F. Yin, F.R. Chen, X.W. Du, Silver clusters with adatoms as a catalyst for the oxygen reduction reaction, *ACS Catal* 13 (2023) 9181–9189.
- [33] F. Luo, A. Roy, M.T. Sougrati, A. Khan, D.A. Cullen, X. Wang, M. Primbs, A. Zitolo, P. Strasser, Structural and reactivity effects of secondary metal doping into iron-nitrogen-carbon catalysts for oxygen electroreduction, *J. Am. Chem. Soc.* 27 (2023) 14737–14747.
- [34] T. Li, Y. Yao, B.H. Ko, Z. Huang, Q. Dong, J. Gao, W. Chen, J. Li, S. Li, X. Wang, Carbon-supported high-entropy oxide nanoparticles as stable electrocatalysts for oxygen reduction reactions, *Adv. Funct. Mater.* 31 (2021) 210561.
- [35] L. Gao, T. Sun, X. Chen, Z. Yang, M. Li, W. Lai, W. Zhang, Q. Yuan, H. Huang, Identifying the distinct roles of dual dopants in stabilizing the platinum-nickel nanowire catalyst for durable fuel cell, *Nat. Commun.* 15 (2024) 508.
- [36] Y.J. Xion, Y.N. Ma, L.L. Zo, S.B. Ha, H. Chen, S. Wang, M. Gu, Y. Shen, L.P. Zhan, Z.H. Xia, J. L. H. Yang, N-doping induced tensile-strained Pt nanoparticles ensuring an excellent durability of the oxygen reduction reaction, *J. Catal.* 382 (2020) 247–255.
- [37] X.R. Zhao, H. Cheng, X.B. Chen, Q. Zhang, C.Z. Li, J. Xie, Ne. Marinkovic, L. Ma, J.C. Zheng, K. Sasaki, Multiple metal–nitrogen bonds synergistically boosting the activity and durability of high-entropy alloy electrocatalysts, *J. Am. Chem. Soc.* 146 (2024) 3010–3022.
- [38] Z. Qiao, C. Wang, Y. Zeng, J.S. Spendelow, G. Wu, Advanced nanocarbons for enhanced performance and durability of platinum catalysts in proton exchange membrane fuel cells, *Small* 17 (2021) 2006805.
- [39] H.W. Park, B.G. Seo, J.W. Shim, N.I. Kim, Y.S. Choi, J.H. Shim, Atomic layer deposited platinum on tungsten oxide support as high performance hybrid catalysts for polymer electrolyte membrane fuel cells, *Appl. Catal. B-Environ.* 337 (2023) 122956.
- [40] M. Li, Z. Zhao, T. Cheng, A. Fortunelli, C.Y. Chen, R. Yu, Q. Zhang, L. Gu, B.V. Merinov, Z. Lin, Ultrafine jagged platinum nanowires enable ultrahigh mass activity for the oxygen reduction reaction, *Science* 354 (2016) 1414–1419.
- [41] J.Y. Park, W.J. Dong, S.M. Jung, Y.T. Kim, J.L. Lee, Oxygen reduction reaction of vertically-aligned nanoporous Ag nanowires, *Appl. Catal. B-Environ.* 298 (2021) 120586.
- [42] L.Y. Zhang, Z.L. Zhao, C.M. Li, Formic acid-reduced ultrasmall Pd nanocrystals on graphene to provide superior electrocatalytic activity and stability toward formic acid oxidation, *Nano Energy* 11 (2015) 71–77.
- [43] Y. Ouyang, H. Cao, H. Wu, D. Wu, F. Wang, X. Fan, W. Yuan, M. He, L.Y. Zhang, C.M. Li, Tuning Pt-skinned PtAg nanotubes in nanoscales to efficiently modify electronic structure for boosting performance of methanol electrooxidation, *Appl. Catal. B-Environ.* 265 (2020) 118606.
- [44] B. Zhang, G. Zhao, B. Zhang, L. Xia, Y. Jiang, T. Ma, M. Gao, W. Sun, H. Pan, Lattice-confined Ir clusters on Pd Nanosheets with charge redistribution for the hydrogen oxidation reaction under alkaline conditions, *Adv. Mater.* 33 (2021) 2105400.
- [45] L.Y. Zhang, T. Zeng, L. Zheng, Y. Wang, W. Yuan, M. Niu, C.X. Guo, D. Cao, C.M. Li, Epitaxial growth of Pt-Pd bimetallic heterostructures for the oxygen reduction reaction, *Adv. Powder Mater.* 2 (2023) 100131.
- [46] H. Ding, P. Wang, C. Su, H. Liu, X. Tai, N. Zhang, H. Lv, Y. Lin, W. Chu, X. Wu, C. Wu, Y. Xie, Epitaxial growth of ultrathin highly crystalline Pt-Ni nanostructure on a metal carbide template for efficient oxygen reduction reaction, *Adv. Mater.* 34 (2022) 2109188.
- [47] B. Lim, M. Jiang, P.H.C. Camargo, E.C. Cho, J. Tao, X. Lu, Y. Zhu, Y. Xia, Pd-Pt bimetallic nanodendrites with high activity for oxygen reduction, *Science* 324 (2009) 1302–1305.
- [48] A.R.C. Bredar, M.D. Blanchet, A.R. Burton, B.E. Matthews, S.R. Spurgeon, R.B. Comes, B.H. Farnum, Oxygen reduction electrocatalysis with epitaxially grown spinel MnFe_2O_4 and Fe_3O_4 , *ACS Catal.* 12 (2022) 3577–3588.
- [49] S.V.P. Vattikuti, P.C. Nagajothi, K.C. Devarayapalli, K. Yoo, N.D. Nam, J. Shim, Hybrid Ag/MoS₂ nanosheets for efficient electrocatalytic oxygen reduction, *Appl. Surf. Sci.* 526 (2020) 146751.
- [50] Z.L. Zhao, L.Y. Zhang, S. Bao, C.M. Li, One-pot synthesis of small and uniform Au@PtCu core-alloy shell nanoparticles as an efficient electrocatalyst for direct methanol fuel cells, *Appl. Catal. B-Environ.* 174 (2015) 361–366.
- [51] Z. Mao, C. Ding, X. Liu, Q. Zhang, X. Qin, H. Li, F. Yang, Q. Li, X.G. Zhang, J. Zhang, Interstitial B-Doping in Pt lattice to upgrade oxygen electroreduction performance, *ACS Catal.* 12 (2022) 8848–8856.
- [52] R. Guo, K. Zhang, Y. Liu, Y. He, C. Wu, M. Jin, Hydrothermal synthesis of palladium nitrides as robust multifunctional electrocatalysts for fuel cells, *J. Mater. Chem. A* 9 (2021) 6196.
- [53] Y. Xiong, Y. Ma, L. Zou, S. Han, H. Chen, S. Wang, M. Gu, Y. Shen, L. Zhang, Z. Xia, N-doping induced tensile-strained Pt nanoparticles ensuring an excellent durability of the oxygen reduction reaction, *J. Catal.* 382 (2020) 247–255.
- [54] Y.N. Chen, X. Zhang, H. Cui, X. Zhang, Z. Xie, X.G. Wang, M. Jiao, Z. Zhou, Synergistic electrocatalytic oxygen reduction reactions of Pd/B₄C for ultra-stable Zn-air batteries, *Energy Stor. Mater.* 15 (2018) 226–233.
- [55] X. Yang, C. Priest, Y. Hou, G. Wu, Atomically dispersed dualmetalsite PGM-free electrocatalysts for oxygen reduction reaction: Opportunities and challenges, *SusMat* 2 (2022) 569–590.
- [56] X. Tian, X. Zhao, Y.Q. Su, L. Wang, H. Wang, D. Dang, B. Chi, H. Liu, E.J. Hensen, X.W.D. Lou, Engineering bunched Pt-Ni alloy nanocages for efficient oxygen reduction in practical fuel cells, *Science* 366 (2019) 850–856.
- [57] B. Zhang, G. Fu, Y. Li, L. Liang, N.S. Grundish, Y. Tang, J.B. Goodenough, Z. Cui, General strategy for synthesis of ordered Pt₃M intermetallics with ultrasmall particle size, *Angew. Chem. Int. Ed.* 59 (2020) 7857–7863.
- [58] J. Zhang, K. Sasaki, E. Sutter, R.R. Adzic, Stabilization of platinum oxygen-reduction electrocatalysts using gold clusters, *Science* 315 (2007) 220–222.
- [59] J. Greeley, I. Stephens, A. Bondarenko, T.P. Johansson, H.A. Hansen, T. Jaramillo, J. Rossmeisl, I. Chorkendorff, J.K. Nørskov, Alloys of platinum and early transition metals as oxygen reduction electrocatalysts, *Nat. Chem.* 1 (2009) 552–556.
- [60] M. Luo, S. Guo, Strain-controlled electrocatalysis on multimetallic nanomaterials, *Nat. Rev. Mater.* 2 (2017) 17059.
- [61] J.K. Nørskov, J. Rossmeisl, A. Logadottir, L. Lindqvist, J.R. Kitchin, T. Bligaard, H. Jonsson, Origin of the overpotential for oxygen reduction at a fuel-cell cathode, *J. Phys. Chem. B* 108 (2004) 17886–17892.
- [62] T. He, W. Wang, F. Shi, X. Yang, X. Li, J. Wu, Y. Yin, M. Jin, Mastering the surface strain of platinum catalysts for efficient electrocatalysis, *Nature* 598 (2021) 76–81.
- [63] J. Zhang, Y. Yuan, L. Gao, G. Zeng, M. Li, H. Huang, Stabilizing Pt-based electrocatalysts for oxygen reduction reaction: Fundamental understanding and design strategies, *Adv. Mater.* 33 (2021) 2006494.